Journal of The Electrochemical Society, **157** (7) K152-K155 (2010)
0013-4651/2010/157(7)/K152/4/$28.00 © The Electrochemical Society

Titania Nanotube Supported Gold Photoanodes for Photoelectrochemical Cells

Peter Aurora,[a,c] Paul Rhee,[b,c] and Levi Thompson[a,b,c,z]

[a]*Department of Mechanical Engineering,* [b]*Department of Chemical Engineering, and* [c]*Hydrogen Energy Technology Laboratory, University of Michigan, Ann Arbor, Michigan 48109-2136,USA*

A major challenge to the use of photoelectrochemical cells for the production of hydrogen from water and solar energy is the low photoanode efficiency. These low efficiencies are largely due to losses associated with the recombination of the charge carriers and low photocatalytic activities. In this work, two strategies were investigated for improving the photoanode performance: producing the semiconducting oxide (TiO_2) in the form of long nanotube arrays and incorporating gold nanoparticles onto the surface. Highly ordered TiO_2 nanotube (TiNT) arrays were fabricated using an anodization process. By varying the conditions, TiNTs with different dimensions were fabricated. Gold nanoparticles with sizes that ranged from 3 to 12 nm were deposited onto selected TiNTs using a modified deposition precipitation method. Increasing the nanotube length resulted in increased photocurrents up to lengths that exceeded the diffusion length of electrons in TiO_2 ($\sim$20 μm). The deposition of gold (Au) nanoparticles resulted in significantly improved electrocatalytic properties. The nonlinear correlation between photocurrent and particle size suggested that sites on the Au nanoparticles were not the most active sites for water oxidation.
 [DOI: 10.1149/1.3417096]

Manuscript received January 28, 2010. Published May 18, 2010.

Photoelectrochemical (PEC) cells are being developed to produce hydrogen and oxygen from water and solar energy. These devices typically consist of a photoanode where water is oxidized and oxygen evolution occurs, a cathode where hydrogen evolution occurs, and an electrolyte. A major obstacle to their use is the low efficiency of the photoanode. By some accounts, the rate of water oxidation at the photoanode needs to be increased by more than an order of magnitude to keep pace with the production of photogenerated charge carriers.[1] In addition, when particulate (powdered) catalysts are used in the photoanode, only about 5% of the generated carriers are available for the reaction;[2] most of the holes and electrons recombine before they can be utilized.

This paper describes research that explored two strategies for improving the performance of the photoanode: producing the oxides in the form of nanotubes to enhance charge transport and reduce recombination losses and incorporating gold nanoparticles to increase the reaction rates. The nanotube architecture should facilitate a more efficient separation and reduce the recombination of photogenerated charge carriers.[3-5] This approach should also improve light harvesting efficiencies due to the high surface areas that can be achieved.

When supported on reducible oxide supports such as TiO_2, gold nanoparticles have been reported to possess extraordinary activities for catalytic reactions including CO oxidation,[6] water–gas shift,[7] and photocatalytic oxidation,[8] and they hold promise for significantly enhancing the water oxidation rates for PEC cells. Previous work has shown that noble metal nanoparticles can also facilitate charge transport in the semiconductor nanostructures and improve charge separation efficiencies by storing charge carriers.[8]

Experimental

Photocatalyst and photoelectrode preparation.— An anodization technique was used to prepare the TiO_2 nanotubes (TiNTs)[3,5] starting with titanium (Ti) foils (Sigma-Aldrich, 99.7% purity, 0.127 mm thickness). Before anodization, the foils were thoroughly cleaned, then dried in air for 30 min at 80°C. The electrolyte consisted of 0.3 wt % NH_4F (Sigma-Aldrich, 98+%) and 98 wt % ethylene glycol (Fisher, less than 0.2 wt % H_2O) in deionized (DI) water. The anodization was performed using a two-electrode cell, where the anode was the Ti foil substrate and the cathode was a Pt foil. The electrodes were connected to a power supply and the voltage was increased from the open circuit to 20–60 V. The as-prepared nanotube arrays were amorphous. These arrays were crystallized via calcination in air at 500°C for 3 h.

Gold was deposited onto the TiNT surfaces using a modified deposition–precipitation method.[9] After calcination, the nanotube arrays were immersed in DI water (6.0 mL) under vigorous stirring. The Au precursor solutions consisted of $HAuCl_4 \cdot 3H_2O$ in DI water; the solution concentration was varied (0.5–2.0 mg/mL) to achieve different Au loadings. The temperature of the solution was maintained at $\sim$50°C. The gold precursor solution was slowly added to the support and the pH of the suspension was maintained between 3 and 10 by adding small amounts of an aqueous solution of Na_2CO_3 (1.0 mg/mL). After the deposition of Au, the substrates were rinsed three to five times with DI water and then transferred to a vacuum oven maintained at 80°C and dried overnight.

For comparison, photoelectrodes were also prepared from TiO_2 powder (P25, Degussa) by depositing a paste of the powder onto a conductive glass substrate. The paste was made by combining P25 with a poly(ethylene glycol) (MW 10,000, Polysciences, Inc.) solution. This paste was deposited onto the substrates using the doctor-blade technique. For the TiNT arrays, the electrodes were prepared by attaching the TiNT film to a glass substrate using a Bisphenol A based epoxy (DeVon 5 Minute Epoxy).

Material characterization.— A scanning electron microscope (Philips XL30), a high resolution transmission electron microscope (TEM, JEOL 3011), and an X-ray diffractometer (XRD, Miniflex, Rigaku) were used to characterize the micro- and nanostructural properties of the materials. The Au loadings were determined using an inductively coupled plasma spectrometer (Varian 710-ES optical emission spectrometer).

To compare the performance of photoelectrodes with different structures, the measured photocurrents were normalized by the geometric area of the electrode (referred to as photocurrent density), total surface area, or Au surface area. The latter two surface areas were measured electrochemically using cyclic voltammetry.[10] The electrochemical surface area measurements were accomplished using a three-electrode cell: The working electrode was the photoanode; the counter electrode was a Pt foil; and a Ag/AgCl (0.199 V_{SHE}) (where SHE is the standard hydrogen electrode) was used as the reference electrode. A reference capacitance of 50 $\mu F/cm^2$ was used to estimate the total surface area based on the double layer capacitance.[1] A reference charge of 390 mC/cm^2 was used to estimate the Au surface area based on the integrated charge under the oxygen adsorption peak.[10] The physical surface areas and

[z] E-mail: ltt@umich.edu

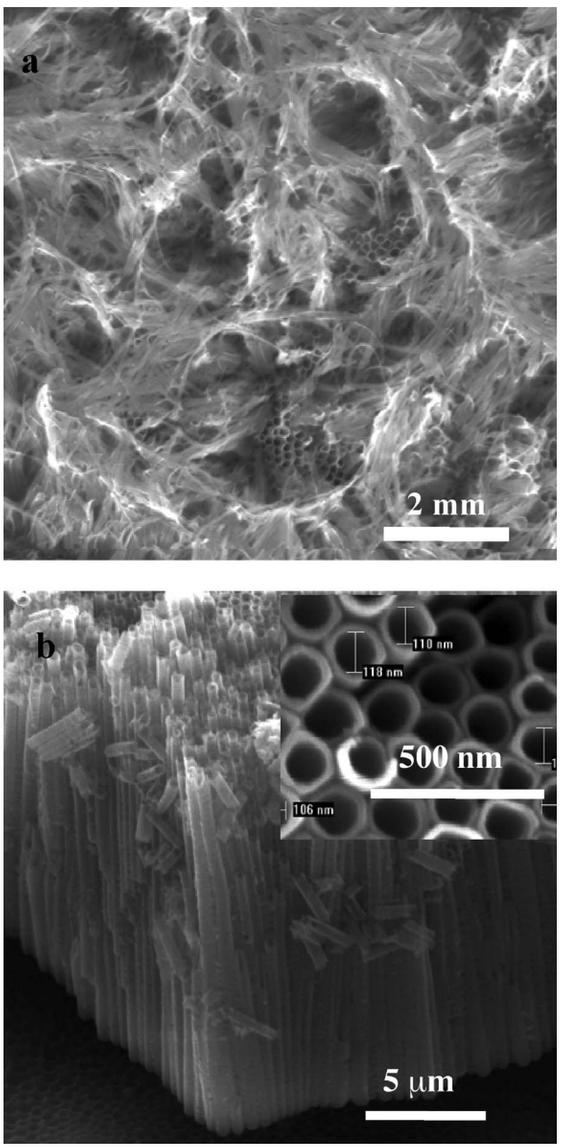

Figure 1. Scanning electron micrographs of the nanotube arrays: (a) As-prepared material before cleaning and (b) material after sonication to remove the debris.

pore size distributions for the powder samples were measured using N_2 physisorption (Micromeritics 2010). The BET surface area for the powder TiO_2 was 54 m^2/g.

PEC performance evaluation.— The PEC measurements were carried out using a three-electrode cell with a Pt foil as the cathode and a Ag/AgCl (0.199 V_{SHE}) reference electrode placed near the anode. The electrolyte was 1.0 M KOH. The cell included a 1 in. diameter quartz window for light incidence. A computer-controlled potentiostat (Gamry Instruments Series G750) was used to control the potential, record the photocurrent, and perform cyclic voltammetry and chronoamperometry. A 300 W solar simulator (Solar Light 16S-300) was used as the light source. This simulator had an AM 1.5 filter that yielded an irradiation output of 100 mW/cm^2 of visible solar light. The intensity of the light was measured using a power and energy meter (Newport Corporation, model 70260).

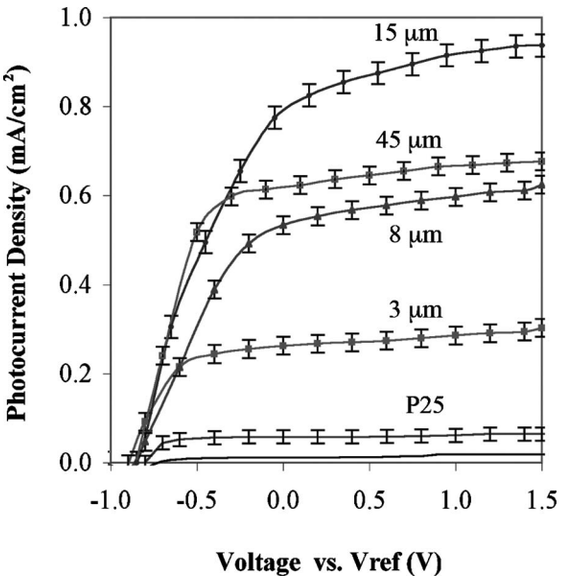

Figure 2. Comparison of *i-V* curves for P25 and TiNT arrays of varying lengths. The TiNT materials were calcined at 500°C. The solid black lines are from measurements taken without light. Simulated sunlight 1.5 was used.

Results and Discussion

Anodization of the Ti foils in fluoride solution resulted in the formation of highly ordered nanotube arrays. Figure 1a illustrates the surface morphology of the as-prepared TiNT films. The debris that covered the top surface was removed via sonication in ethanol for 3 min. Figure 1b illustrates the typical morphology of the nanotube films after the cleaning procedure; the inset is a scanning electron micrograph of the nanotube array cross section. By varying the anodization conditions, TiNTs with different dimensions were fabricated. The outer diameter, wall thickness, and length ranged from 60 to 200 nm, 10 to 50 nm, and 3 to 75 μm, respectively.

XRD patterns indicated that the as-prepared TiNTs were amorphous. Annealing the nanotube arrays resulted in the transformation of the amorphous material primarily into anatase TiO_2. The photocatalytic properties of TiO_2 depend on its crystallinity and phase. The anatase phase is typically preferred for electrochemical applications over the rutile phase because the anatase phase appears to be more active for water oxidation.[5,11] Differences between the phases could be a consequence of the differing conduction band (CB) energies. The CB energy (E_{CB}) for rutile TiO_2 is essentially coincident with the reversible hydrogen potential at all pH values, whereas for anatase TiO_2, the E_{CB} is more negative by 0.20 V. Also, anatase exhibits higher electron mobility, lower dielectric constant, and lower deposition temperature than rutile,[11] which makes it more attractive for solar light applications. There were small peaks in the XRD patterns associated with the rutile phase. These may have been due to material under the nanotube arrays. Mor et al.[3] reported, based on high resolution transmission electron microscopy and energy-dispersive X-ray spectroscopy results, that the nanotube walls were anatase, whereas the underlying oxide was rutile.

Figure 2 shows the photocurrent density as a function of voltage (*i-V*) for several different photoelectrodes. The solid black lines were taken without light. The photocurrents increased with increased tube length up to a limit. The increase may have been a consequence of increased light absorption and active site densities for water oxidation due to the higher surface areas. It has also been argued that the tube structure can enhance the transport of electrons before the recombination with holes, leading to higher photocurrent densities.[3-5,12] Although TiNTs longer than 75 μm were readily produced, the results indicate that there was no performance benefit

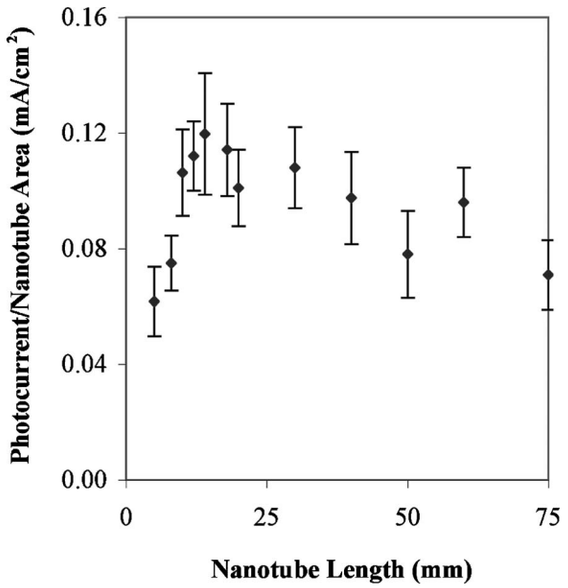

Figure 3. The photocurrent normalized by the total electrochemical surface area as a function of nanotube length with applied potential of 40 V. The nanotube films were calcined at 500°C for 3 h.

associated with using tubes longer than 15–20 μm (Fig. 3). The diffusion length of electrons in long TiNTs is 15–20 μm, suggesting that for tubes longer than this length, charge carriers could recombine before participating in reactions.[12,13] Also, due to shadowing, the light might not be able to reach the bottom of the nanotubes; therefore, producing tubes longer than ~20 μm could lead to inefficiencies. Similar results have been reported by Lynch et al.[12] Furthermore, electrolyte mass-transport limitations could hinder performance for the longer nanotubes. Based on these results, tubes with average lengths of ~15 μm were used for most of the experiments.

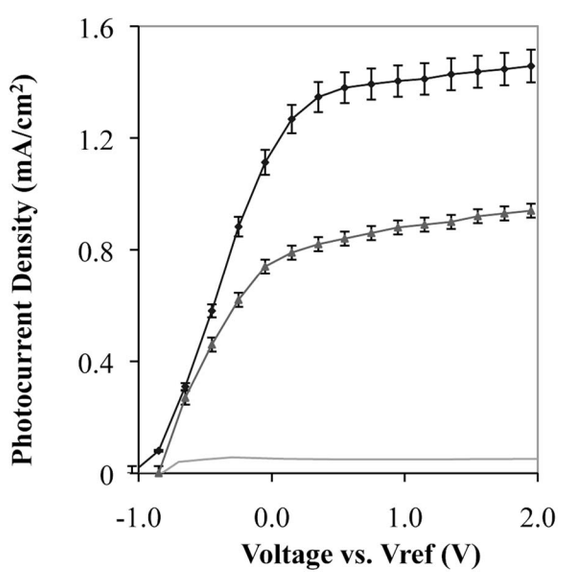

Figure 4. Photocurrent density-voltage curves for TiNT (solid triangles) and Au/TiNT electrodes (solid circles). Measurements in the dark are indicated by the bottom line. The nanotubes were calcined at 500°C and had lengths of 15 μm and outer diameters of 140 nm. The Au loading was 1.3 wt %, and the average Au particle size was 4.2 nm.

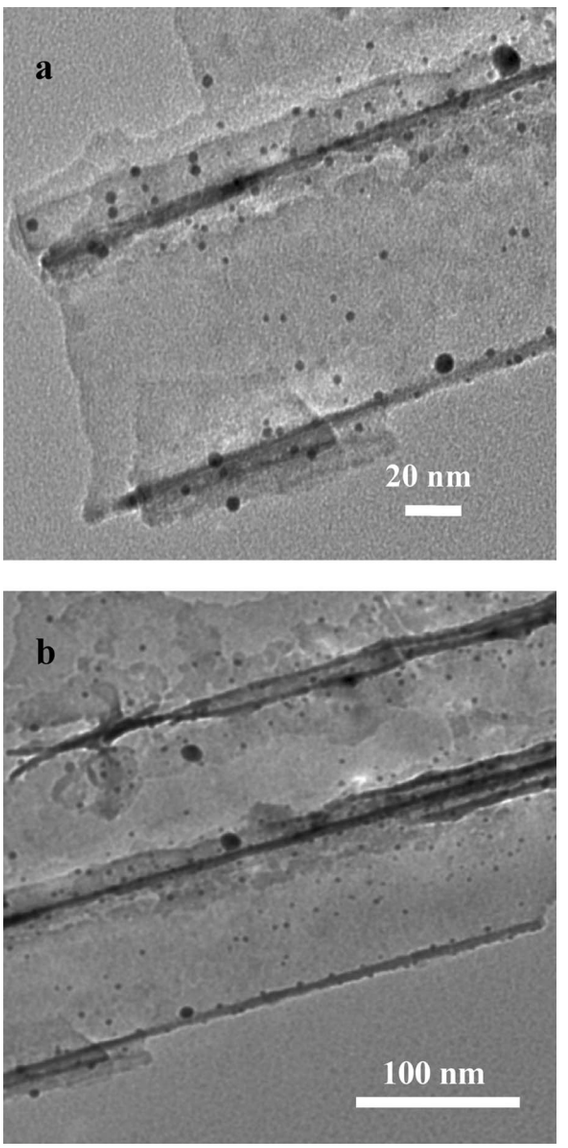

Figure 5. Transmission electron micrographs of the Au/TiNT photocatalysts. The average nanotube outer diameter was 140 nm. The Au loadings were (a) 0.8 and (b) 1.2 wt %.

The addition of Au to the TiNTs caused an increase in the photocurrent. Figure 4 shows the *i-V* plots for selected TiNT and Au/TiNT electrodes (nanotube length 15 μm and outer diameter 140 nm). The Au loading was 1.3 wt % and the average Au particle size was 4.2 nm. The photocurrent density produced by the Au/TiNT electrode (at 0.5 V bias voltage) was ~70% higher than that for the TiNT alone. This increase could be due to an increase in the photocatalytic activity and/or a decrease in the bandgap. Although the surface of massive gold exhibits modest catalytic properties, Au nanoparticles can be highly active.[14] As the Au particle size decreases, the proportion of atoms at or close to the surface increases. Subramanian and co-workers[8] have shown that the performance of Au/TiO_2 powder based photoelectrodes varied significantly with Au particle size. Typically, the photocurrent increased with decreasing Au particle size.

In an attempt to understand the basis for the improved activity that resulted from adding Au nanoparticles, we measured the total and Au electrochemical surface areas of electrodes with a range of Au loadings and particle sizes. The Au loadings ranged from 0.2 to

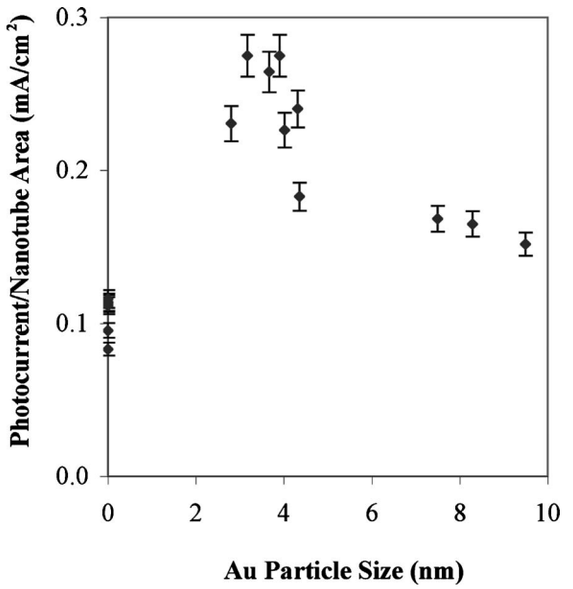

Figure 6. The total electrochemical surface area normalized photocurrent as a function of average Au particle size. The length and outer diameter for the TiNTs were 15 μm and 140 nm, respectively.

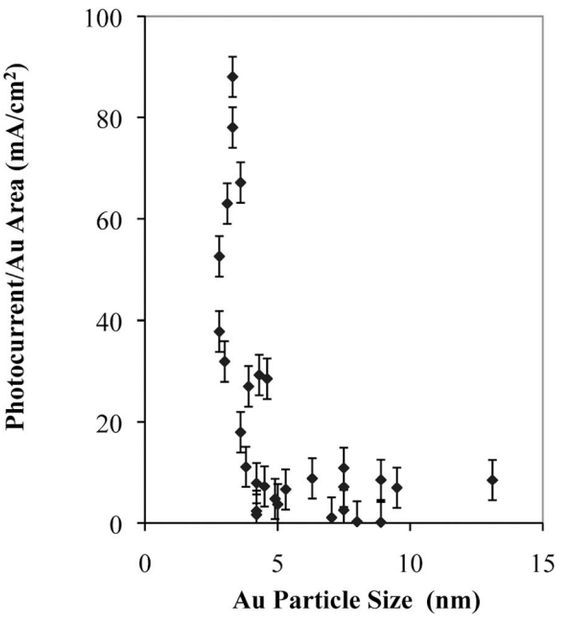

Figure 7. The Au electrochemical surface area normalized photocurrent as a function of average Au particle size. The length and outer diameter for the TiNTs were 15 μm and 140 nm, respectively.

3.5 wt %. Figure 5 shows two TEM micrographs for the TiNT supported Au photoelectrodes. The surfaces contained relatively high densities of particles with sizes ranging from 3 to 12 nm. Figure 6 illustrates the photocurrent normalized by the total electrochemical surface area as a function of the Au average particle size. The Au loadings for these materials were typically 1.2–1.7 wt %. The maximum specific photocurrent was obtained for films containing Au nanoparticles between 4 and 5 nm. These results indicate that sites associated with the Au nanoparticles contributed significantly to the water oxidation activity, and that the activity was influenced by the Au particle size. A variety of sites could be associated with the Au nanoparticles: sites on the nanoparticles, sites at the nanotube–nanoparticle interface, and/or sites on TiO_2 that were modified by Au.

The Au electrochemical surface area normalized photocurrents increased dramatically as the size of the Au nanoparticles decreased below ~5 nm (Fig. 7). Assuming that the electrochemical measurements are done on the sample sites on Au nanoparticles, the nonlinear correlation illustrated in Fig. 7 suggests that sites on the Au nanoparticles were not the most active sites for water oxidation. The specific rate for CO oxidation[6] has also been reported to increase dramatically for Au nanoparticles smaller than ~4 nm. Bond and Thompson suggested that the increased activities were due to a combination of effects: loss of metallic character, changes in particle morphology, and stronger interactions between Au and the support.[14] On-going characterization work should help us understand the basis for the dramatic increase in photocurrent on decreasing the Au particle size.

Conclusion

Photocurrents for TiNT photoanodes increased with increases in the nanotube length up to ~20 μm. This observation was attributed to the enhanced capture of the light and better separation of the charge carriers. The incorporation of Au nanoparticles significantly improved the rates for water oxidation. As the Au nanoparticle size decreased, the photocurrent increased, suggesting that Au introduced highly active sites to the TiNTs. Experiments are underway to determine the structural and compositional character of active sites involved in H_2O oxidation.

Acknowledgments

The authors acknowledge the Hydrogen Energy Technology Laboratory for the financial support, the staff at the Electron Microbeam Analysis Laboratory for assistance, and Professor Volker Sick for advice regarding this work.

University of Michigan assisted in meeting the publication costs of this article.

References

1. N. S. Lewis and G. Crabtree, Report of the Basic Energy Sciences Workshop on Solar Utilization, Office of Science, U.S. Department of Energy (2005).
2. P. V. Kamat, *J. Phys. Chem. C*, **111**, 2834 (2007).
3. G. K. Mor, O. K. Varghese, M. Paulose, K. Shankar, and C. A. Grimes, *Sol. Energy Mater. Sol. Cells*, **90**, 2011 (2006).
4. K. Shankar, J. I. Bashman, N. K. Allen, O. K. Varghese, G. K. Mor, X. Feng, M. Paulose, J. A. Seabold, K. Choi, and C. A. Grimes, *J. Phys. Chem. C*, **113**, 6327 (2009).
5. A. Ghicov and P. Schmuki, *Chem Commun. (Cambridge)*, **2009**, 2791.
6. M. Haruta and M. Date, *Appl. Catal., A*, **222**, 427 (2001).
7. C. H. Kim and L. T. Thompson, *J. Catal.*, **244**, 248 (2006).
8. V. Subramanian, E. E. Wolf, and P. V. Kamat, *J. Am. Chem. Soc.*, **126**, 4943 (2004).
9. C. H. Kim and L. T. Thompson, *J. Catal.*, **230**, 66 (2005).
10. S. Trasatti and O. A. Pettri, *J. Electroanal. Chem.*, **327**, 353 (1992).
11. A. Fujishima, X. Zhang, and D. A. Tryk, *Surf. Sci. Rep.*, **63**, 515 (2008).
12. R. P. Lynch, A. Ghicov, and P. Schmuki, *J. Electrochem. Soc.*, **157**, G76 (2010).
13. A. C. Fisher, L. M. Peter, E. A. Ponomarev, A. B. Walker, and K. G. U. Wijayantha, *J. Phys. Chem. B*, **104**, 949 (2000).
14. *Catalytic Science Series*, G. C. Bond, C. Louis, and D. T. Thompson, Editors, Vol. 6, Imperial College Press, London (2006).